On-Chip Solc-Type Polarization Control and Wavelength Filtering Utilizing Periodically Poled Lithium Niobate on Insulator Ridge Waveguide

Tingting Ding, Yuanlin Zheng, and Xianfeng Chen

***Abstract*—The state-of-the-art lithium niobate on insulator technology has enabled a variety of fascinating integrated functionalities. It combines versatile properties of lithium niobate and a high refractive index contrast of it with respect to silica or air for integrated photonic applications. Here, we present an on-chip Solc-type device based on transverse electro-optic effect at the telecommunication wavelengths in a periodically poled lithium niobate on insulator ridge waveguide. The efficient quasi-phase matched TE↔TM mode converter controlled by transverse applied electric field at low voltages is demonstrated for both linear polarization rotation and wavelength filtering at fast modulation speed. This paper demonstrates promises for developing novel integrated devices on the new platform for polarization sensitive applications.**

***Index Terms*—Electro-optic, lithium niobate on insulator, ridge waveguide, Solc-type device.**

I. Introduction

As a versatile crystal, lithium niobate (LN) is widely used for various electro-optic (EO) and nonlinear applications in both bulk and integrated devices for its wide transparent range, large EO and nonlinear coefficients. Recently, the emerging lithium niobate on insulator (LNOI) technology has attracted much interest, which provides a unique platform for integration of excellent properties of lithium niobate (LN) [1] for optical processing and light-matter interaction enhancement on a chip. Thus, exploiting these favorable properties in photonic integrated circuits (PICs) is becoming popular in a wide range of applications, and extensive research has been put forth to demonstrate multi-functional devices on LNOI in the past years. Prominent examples on nano LNOI films include on-chip waveguide modulators [2]–[5], microresonators [6]–[10], and frequency converters [11]–[14], which exploits the excellent optical confinement for highly efficient wave mixing using small applied voltages or input powers.

However, the realization of the most desired quasi-phase-matching (QPM) schemes in nano LNOI films is still in its infancy [14]–[16], due to difficulty in fabricating stable QPM gratings in LNOI films or waveguide structures in PPLNOI films. An alternative way is to utilize micrometer thick PPLNOI films, typically obtained by mechanical thinning method. Then, waveguide structures can be fabricated via optical grade dicing other than etching methods. They are also appealing in various applications, which has been implemented for nonlinear frequency conversion, such as second-harmonic generation (SHG) [17], [18], high-harmonic generation (HHG) [19], and optical parametric amplification (OPA) [20]. The development of PPLNOI ridge waveguides is particularly attractive, because it allows the realization of on-chip QPM devices.

Electro-optic (EO) effect induced wave coupling can also benefit from such compact configuration for low voltage drive and high-speed operation. The scheme has been demonstrated to realize many important applications in optical communications (often with high voltage drive and slow response), such as narrow-band tunable Solc filters, ultra-precision polarization generator and optical delay lines [21]–[23]. Mode conversion has been reported in Ti:PPLN waveguides [24], where both TE and TM modes are supported. (The proton exchanged LN waveguide only supports TM modes, thus principally preventing it from mode conversion applications.) There is a great advantage for LNOI in light confinement for highly dense photonic integration over such conventional LN waveguides. Note that there has been over 40-GHz EO modulators on LNOI platform [2], [3], [25], but no mode conversion was involved without QPM for TE↔TM mode coupling. Optical elements that can control the polarization of light in LNOI optical circuits are important [1], as optical properties of LN are polarization sensitive. As mentioned above, the realization of QPM schemes to achieve this goal on the LNOI platform is intriguing, but until now, few report focuses on the transverse EO effect in PPLNOI ridge waveguide structure for active mode conversion and its application demonstration.

In this work, we describe the fabrication and demonstration of PPLNOI ridge waveguides in the configuration of an on-chip Solc-type scheme for TE↔TM mode conversion for polarization control and wavelength filtering, with the advantages of

Manuscript received September 18, 2018; revised December 16, 2018; accepted January 8, 2019. Date of publication January 10, 2019; date of current version February 22, 2019. The work was supported in part by the National Natural Science Foundation of China (NSFC) under Grants 11604206 and 11734011; in part by the National Key R&D Program of China under Grants 2018YFA0306301 and 2017YFA0303701; in part by Shanghai Municipal Education Commission (16CG08); and in part by the Foundation for Development of Science and Technology of Shanghai (17JC1400400). *(Corresponding authors: Yuanlin Zheng and Xianfeng Chen.)*

The authors are with the State Key Laboratory of Advanced Optical Communication Systems and Networks, School of Physics and Astronomy, Shanghai Jiao Tong University, Shanghai 200240, China (e-mail: dtt1994@sjtu.edu.cn; ylzheng@sjtu.edu.cn; xfchen@sjtu.edu.cn).

Color versions of one or more of the figures in this paper are available online at http://ieeexplore.ieee.org.

Digital Object Identifier 10.1109/JLT.2019.2892317

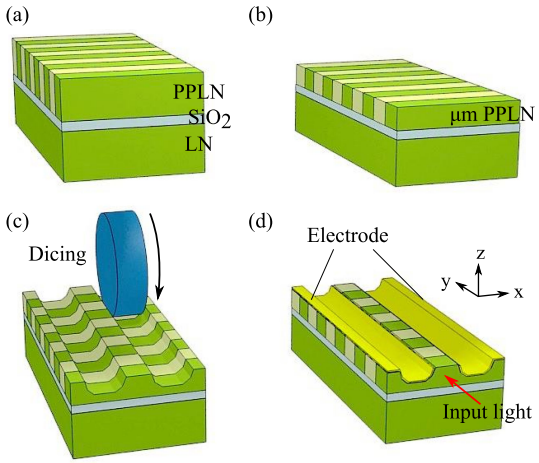

Fig. 1. Flow chart illustration of the PPLNOI ridge waveguide fabrication. (a) Bonding of PPLN onto a silica layer on a LN substrate; (b) Chemical-mechanical thinning to achieve the micro thick PPLNOI layer; (c) Optical grade dicing of two grooves in the PPLNOI layer to form the ridge waveguide in between; (d) Deposition of electrodes on both sides of the ridge waveguide. A buffer silica layer was introduced to reduce absorption by the metallic electrodes.

integration, low drive voltage, wide operational wavelength, and potentially high speed response.

II. Experiment and Discussion

The fabrication of the PPLNOI ridge waveguide (in collaboration with *HC Photonics Corp.*) is broken down into four primary steps: (1) bonding a PPLN chip with the pre-deposit silica layer on another LN substrate, (2) thinning of the bonded PPLN layer to micrometer thick using the chemical-mechanical polishing method, (3) optical grade dicing to fabricate high-quality grooves between which the ridge waveguide is formed, and (4) electrode depositing. The fabrication procedure of the ridge waveguide is schematically outlined in Fig. 1. The poling period of the PPLN is 20.5 μm with a duty cycle of 50%, which was designed to fulfill QPM in PPLN in the telecommunication band. The thinned LNOI layer has a thickness of approximately 5.0 μm. Two parallel shallow grooves, whose depth is approximately 2.5 μm, are cut by the diamond precision dicing method [26], [27]. The ridge structure with a respective height and width of 5.0 and 6.0 μm is formed in between the two. Wedged sidewalls are inevitable during swallow dicing. A hundreds nanometer thick Silica buffer layer is deposited on top. Then, metallic (Ni/Cr) electrodes are deposited to form the transverse electrodes. The thickness of the electrodes is approximately 50 nm. The length of the waveguide is 10 mm. The width of the PPLNOI chip is 1.5 mm only. The thickness of the LN substrate is 1.0 mm.

The TE↔TM mode conversion mechanism in the PPLNOI ridge waveguide is similar with that in bulk PPLN experiencing transverse EO effect [22]. When applied a transverse (x axis) electric field along a PPLN crystal, its optical axis of each positive and negative domain is alternately re-aligned at a small angle of θ and $-\theta$ around the y axis, mimicking the structure of a folded Solc-type filter. The rocking angle θ is proportional to the applied electric field intensity, E, and has the

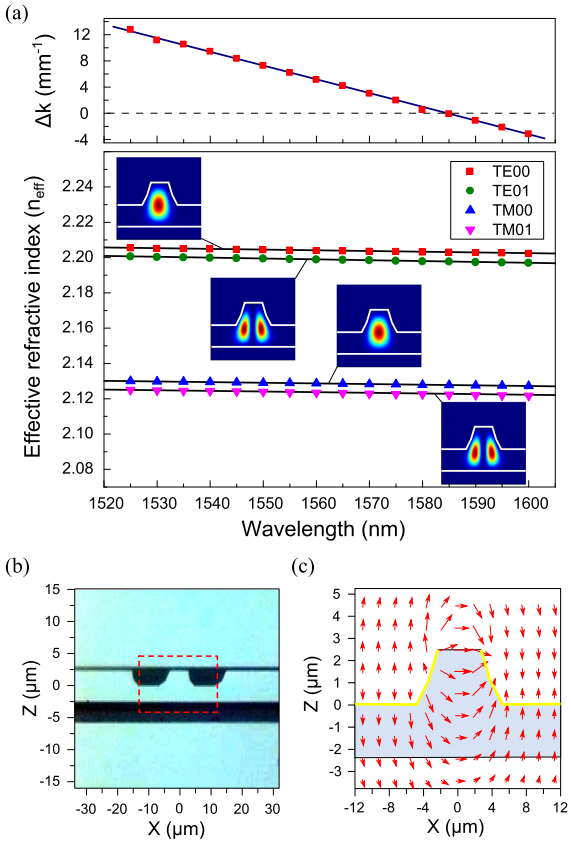

Fig. 2. (a) Calculated dispersion of the supported modes, and the vector mismatching between the fundamental modes of TE00 and TM00 in the PPLNOI ridge waveguide. (b) Image of the ridge waveguide's cross section. (c) Cross-section view of the simulated electrical field.

form of $\theta \approx \gamma_{51} E/[(1/n_e)^2 - (1/n_o)^2]$, where γ_{51} is the EO coefficient, n_e, n_o are the extraordinary and ordinary refractive indices, respectively. Meanwhile, The operating wavelength λ, satisfying the QPM condition, is given by $\lambda = \Lambda(n_o - n_e)$, where Λ is the poling period of the PPLN. At the QPM wavelength, the polarization of the output is rotated by an angle of $2N\theta$, where N is the domain number. The linear polarization state of light is maintained in this configuration, which in true is a linear polarization rotator [22]. Meanwhile, the QPM wavelength is sensitive to temperature variation, i.e., the operating wavelength can be tuned via temperature control. The scenario in waveguide structures is similar, but the reduced transverse dimension, as compared with bulk LN devices, enables a dramatic increase in the modulation field intensity per applied voltage. High-speed modulation is possible, which is a direct benefit of the LNOI platform. It is worth to notice that polarization converters or switches in homogeneous EO media, which rely on the modulation of the relative phase shift between TE and TM modes (the EO retardation), can only preserve linear polarization at two orthogonal eigen modes. At other phase retardation, the output polarization is either elliptical or circular.

Due to a large cross-section and high refractive index contrast, the ridge waveguide is found to support multiple eigen modes, i.e., highly multimode. Thus, it is necessary to consider possible coupling between different spatial modes. Fig. 2(a) shows the

calculated dispersion of the ridge waveguide and phase mismatching at the telecom band range at room temperature, using a finite element mode solver. The insets are the corresponding intensity profiles of the supporting modes. The first two lowest order modes (TE00, TE01, TM00 and TM01) within the wavelength range are presented. The mode overlapping integral of the first and second orders is nearly zero. Moreover, it is also phase mismatched within the wavelength range. Thus, the existence of second-order modes would have little effect on the coupling of fundamental TE/TM modes. Higher order mode coupling is prohibited for the same reason. This is also proved during the experiment, where only one QPM condition is met during the whole laser scanning range. The device is designed to investigate polarization coupling at low drive voltage and high speed. The coupling efficiency is determined both by the overlapping of the optical modes and their overlap with the electrical field. As can be seen, the two modes can be nearly spatially overlapped. The simulated modes have a modal overlap of 0.998, which guarantees pure polarization in spatial dimensions after the collimated output in free space. The simulation predicts the QPM wavelength at about 1585 nm, where the effective wavevector mismatch, $\Delta k = k_o - k_e$, crosses the zero line (horizontal dashed line in Fig. 2(a)). The cross section of an end facet of the fabricated PPLNOI ridge waveguide is shown in Fig. 2(b), with the ridge structure marked by the rectangle. To maximize the in-plane electric field (E_x) and minimize the electrode gap, the electrodes are deposited on the sidewalls of the ridge waveguide. The electrode on each side is fabricated by mounting the chip sample at a large tilt angle during the vapor deposition. The numerically simulated profile of the electric field is given in Fig. 2(c). The electric field is mainly along the x axis at the waveguide center where the mode has the highest intensity. There is also a proportion of the electric field component along the z axis (inevitably due to wedged side walls), but this has little influence on the wave coupling. The induced effect (only refractive index change) are overall canceled out, since the electro-optic coefficient flips sign in the positive and negative domains.

We first show the linear polarization rotation characteristics of our device with efficient and linear EO tuning. The experimental setup is shown in Fig. 3(a). A tunable telecom laser (1520–1600 nm) is used as the light source, the polarization of which is controlled by a polarization controller (PC). An in-line polarization beam splitter (PBS) is placed before the device to guarantee high extinction ratio of the linearly polarized input light. The waveguide is coupled via a pigtail polarization maintaining (PM) fiber, which connects the in-line PBS and the waveguide. The input light is kept either TE or TM polarized. The injecting light power, measured after the in-line PBS, is 1.0 mW to avoid laser induced thermal effect in the waveguide to drift the QPM wavelength, although much higher power can be injected into the ridge waveguide without damaging. The sample is temperature controlled using a TEC chip with an accuracy of 0.1 °C. The package of our device is shown in the photograph in Fig. 3(b), the functional component is actually placed in the end part of the housing, as marked by the red rectangle in the enlarged image. The output is collimated by a

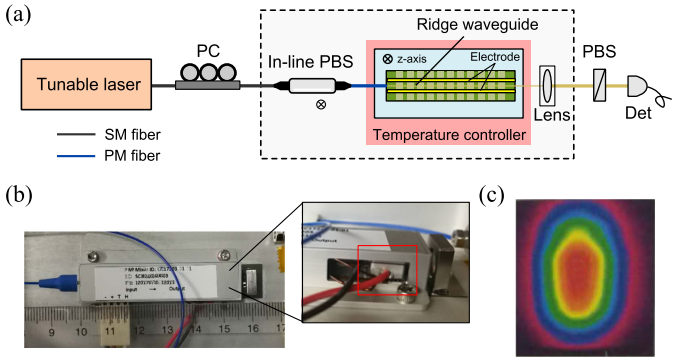

Fig. 3. (a) Experimental setup. PC: polarization controller; PBS: polarization beam splitter; Det: Detector. (b) Package of our device. The ridge waveguide chip is in the red rectangle in the enlarged image. (c) Intensity profile of the spatial collimated output beam in free space.

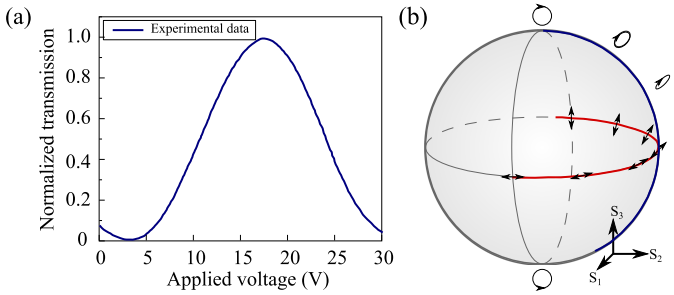

Fig. 4. (a) The output light intensity versus the applied electrical voltage. (b) The output polarization state evolution represented on a Poincaré sphere as the applied voltage increases from 0 to 18 V. Red curve: QPM condition, blue curve: phase mismatched condition.

short focal-length lens to free space, whose measured profile (approximately 2.8×1.9 mm^2) is displayed in Fig. 3(c). The overall loss, including the fiber-waveguide coupling and propagation loss, is 3.5 dB at the L-band wavelengths. The propagation loss is estimated to be approximately 0.3 dB/cm, which indicates smooth sidewalls of the ridge waveguide. The mode mismatch during coupling between the fiber and the waveguide is believed to result in the main loss.

The actual QPM wavelength measured at room temperature is 1595 nm, slightly different from the theoretical prediction. The modulation of the output versus the applied voltage measured after an orthogonal cubic PBS is shown in Fig. 4(a). The half-wave voltage is 13 V. Thus, the voltage-length product of our device is 13 Vcm, and is in agreement with similar research [28]. The theoretical prediction of the voltage is approximately 5 V assuming a rectangular cross-section of the PPLNOI waveguide. The existence of an offset angle at zero voltage may attribute to the strain-optic effect introduced during the slicing process. This can easily be compensated by applying a negative balancing voltage. Fig. 4(b) shows the polarization state of the output at 1595 nm and 1550 nm with respect to the applied voltage, corresponding to QPM and phase mismatching conditions. The replot of the trajectory of polarization evolution measured using a polarimeter is presented on a Poincaré sphere. As can be seen, the polarization evolution takes different paths for the two cases. In the Solc configuration at 1595 nm, the polarization remains

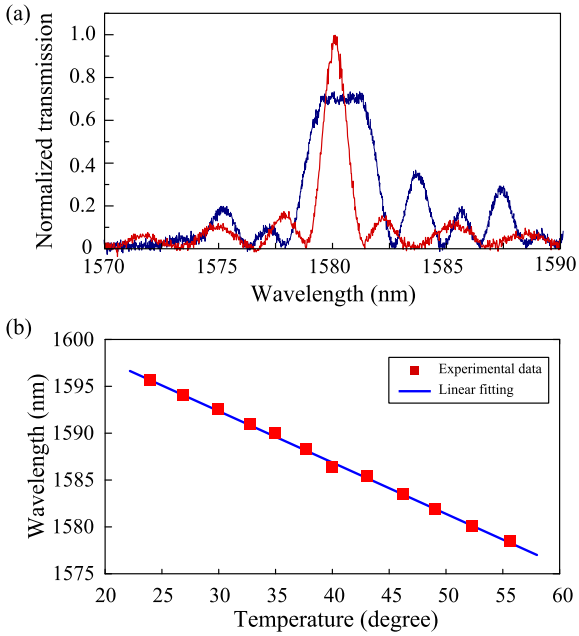

Fig. 5. (a) The Solc transmission spectra measured at 1580 nm at the half-wave voltage (red curve) and beyond (blue curve). (b) The QPM wavelength tuned by temperature.

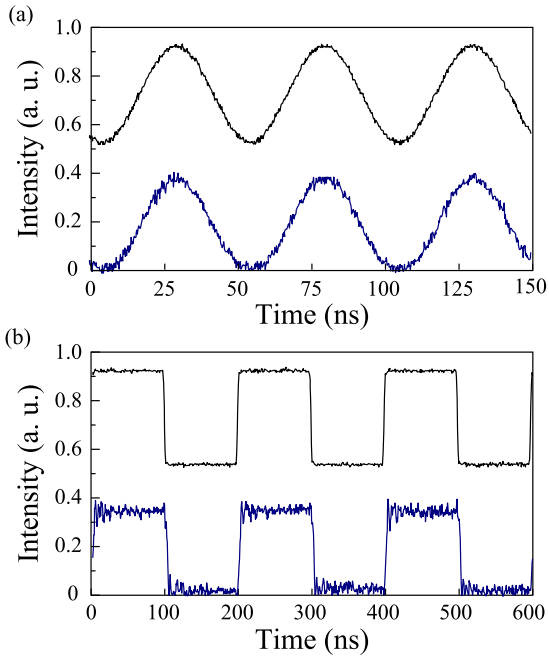

Fig. 6. Time traces of transmitted light operating at MHz driving using (a) sinusoidal and (b) square function signals. Black lines: applied voltage; blue lines: transmission.

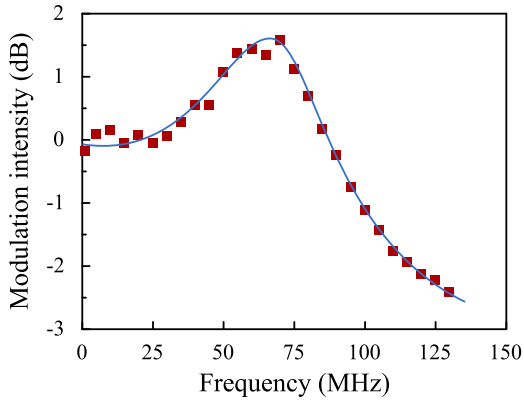

Fig. 7. The frequency response of the device.

on the equatorial plane as the applied voltage varies, indicating the linear polarization at all rotation angles. The rotation angle of the linearly polarized output is measured to be in a good linear relation with the applied voltage. The sinusoidal lineshape of the modulated transmission is also a prove. The device is measured to exhibits a polarization extinction ratio of over 20 dB at each rotation angle. While in the condition much far away from phase matching (e.g. 1550 nm), the polarization evolution of a circularly polarized input light takes a longitudinal path on the Poincaré sphere. The polarization is evolving due to the EO retardation between the eigen TE and TM modes. And, at most times, the polarization is elliptical.

The device can also be used for narrow bandwidth wavelength filtering, since the polarization conversion is strongly wavelength selective, which is the main function of a Solc filter. The red curve in Fig. 5(a) is the transmission spectrum measured after the cubic PBS on the input wavelength at the applied voltage of 18 V, measured at 52 °C. The QPM wavelength is centered at 1580 nm with a 2.4-nm bandwidth at full width at half maximum (FWHM), in good agreement with the calculated result of 2.3 nm using the function of $sinc(\Delta kL/2)$, where Δk is the wavevector mismatch and L is the length of the PPLNOI waveguide. The attractive flat-top transmission, blue curve in Fig. 5(a), is achieved at the critical voltage of 27 V. Detail investigation of this feature can be found elsewhere [29], [30]. This is useful in wavelength filtering to withstand temperature fluctuations. Fig. 5(b) shows the QPM wavelength with temperature, showing a good linear dependence with a sensitivity of $d\lambda/dT \approx -0.5$ nm/°C. Overall, the static performance of our device is in consistence with the design.

Other than the dramatic reduction in driving voltages, another straightforward benefit of using compact structure is fast operation. Fig. 6 shows the time trace of transmitted light after an orthogonal cubic PBS using sinusoidal and square function drive at MHz range (dynamical operation). An offset voltage of 3 V has been added. The shown traces are measured at the frequency of, for instance, 20 MHz and 5 MHz for sinusoidal and square signal drive, as shown in Figs. 6(a) and 6(b), respectively. This shows the ability of our device to continuously rotate and switch light polarization at dynamical operation.

The frequency response of the EO modulator was measured using swept-frequency technique. Fig. 7 shows the experimentally measured result of the relative modulation depth with respect to the electrical frequency. The device has a 3-dB modulation bandwidth of approximately 125 MHz, and a resonance peak at approximately 70 MHz. Although the modulation speed is not surprisingly high at present, the successful demonstration of EO modulator in PPLNOI ridge waveguide is convincing. The recently developed ultrahigh speed phase modulators in

LNOI nanofilms has push this limit to 100 GHz. This is firstly achieved due to lower half-wave voltage for rf driving, and small dimensions for small intrinsic capacity of electrodes, and impedance matching by proper design of the electrodes. The limitation on the modulation speed in our device is mainly due to large capacity and mismatched impedance of the electrodes. The capacity of the electrodes is measured to be 25 pF, and the ohmic resistance (much larger than 50 Ω) is also too large, while ultrahigh-speed EO modulators requires that the electrode capacity be typically smaller than 3 pF/cm and the velocities of optical and RF drive waves be matched. The problem can be overcome by properly designing the narrow rf electrodes and fabrication [2], as will be investigated in the future.

III. Conclusions

In summary, we have developed an on-chip Solc-type device based on PPLNOI ridge waveguide structure. With moving to a LNOI platform and ridge waveguide configuration, an active mode converter with reduced voltage and high speed operation is obtained. We have shown that this scheme is promising for both polarization rotation and wavelength filtering for integrated device application.

References

[1] A. Boes, B. Corcoran, L. Chang, J. Bowers, and A. Mitchell, "Status and potential of lithium niobate on insulator (LNOI) for photonic integrated circuits," *Laser Photon. Rev.*, vol. 6, no. 4, 2018, Art. no. 1700256.

[2] C. Wang, M. Zhang, B. Stern, M. Lipson, and M. Lončar, "Nanophotonic lithium niobate electro-optic modulators," *Opt. Express*, vol. 26, no. 2, pp. 1547–1555, 2018.

[3] A. J. Mercante, P. Yao, S. Shi, G. Schneider, J. Murakowski, and D. W. Prather, "110 GHz CMOS compatible thin film $LiNbO_3$ modulator on silicon," *Opt. Express*, vol. 24, no. 14, pp. 15590–15595, 2016.

[4] M. R. Escalé, D. Pohl, A. Sergeyev, and R. Grange, "Extreme electro-optic tuning of Bragg mirrors integrated in lithium niobate nanowaveguides," *Opt. Lett.*, vol. 43, no. 7, pp. 1515–1518, 2018.

[5] S. Jin, L. Xu, H. Zhang, and Y. Li, "$LiNbO_3$ thin-film modulators using silicon nitride surface ridge waveguides," *IEEE Photon. Technol. Lett.*, vol. 28, no. 7, pp. 736–739, Apr. 2016.

[6] L. Chen, Q. Xu, M. G. Wood, and R. M. Reano, "Hybrid silicon and lithium niobate electro-optical ring modulator," *Optica*, vol. 1, no. 2, pp. 112–118, 2014.

[7] J. Wang *et al.*, "High-Q lithium niobate microdisk resonators on a chip for efficient electro-optic modulation," *Opt. Express*, vol. 23, no. 18, pp. 23072–23078, 2015.

[8] C. Wang *et al.*, "Integrated high quality factor lithium niobate microdisk resonators," *Opt. Express*, vol. 22, no. 25, pp. 30924–30933, 2014.

[9] J. Lin *et al.*, "Fabrication of high-Q lithium niobate microresonators using femtosecond laser micromachining," *Sci. Rep.*, vol. 5, 2015, Art. no. 8072.

[10] T. Wang, P. Chen, W. Hsiao, and C. Chen, "High-Q $LiNbO_3$ microtoroid resonators," *J. Lightw. Technol.*, vol. 34, no. 14, pp. 3306–3311, Jul. 2016.

[11] A. Rao *et al.*, "Second-harmonic generation in periodically-poled thin film lithium niobate wafer-bonded on silicon," *Opt. Express*, vol. 24, no. 26, pp. 29941–29947, 2016.

[12] C. Wang *et al.*, "Second harmonic generation in nano-structured thin-film lithium niobate waveguides," *Opt. Express*, vol. 25, no. 6, pp. 6963–6973, 2017.

[13] P. Mackwitz, M. Rüsing, G. Berth, A. Widhalm, K. Müller, and A. Zrenner, "Periodic domain inversion in x-cut single-crystal lithium niobate thin film," *Appl. Phys. Lett.*, vol. 108, 2016, Art. no. 152902.

[14] L. Chang, Y. Li, N. Volet, L. Wang, J. Peters, and J. E. Bowers, "Thin film wavelength converters for photonic integrated circuits," *Optica*, vol. 3, no. 5, pp. 531–535, 2016.

[15] G. Li, Y. Chen, H. Jiang, and X. Chen, "Broadband sum-frequency generation using d_{33} in periodically poled $LiNbO_3$ thin film in the telecommunications band," *Opt. Lett.*, vol. 45, no. 5, pp. 939–942, 2017.

[16] G.-H. Shao *et al.*, "Ferroelectric domain inversion and its stability in lithium niobate thin film on insulator with different thicknesses," *AIP Adv.*, vol. 6, 2016, Art. no. 075011.

[17] S. Kurimura, Y. Kato, M. Maruyama, Y. Usui, and H. Nakajima, "Quasi-phase-matched adhered ridge waveguide in $LiNbO_3$," *Appl. Phys. Lett.*, vol. 89, 2006, Art. no. 191123.

[18] M. Chauvet *et al.*, "High efficiency frequency doubling in fully diced $LiNbO_3$ ridge waveguides on silicon," *J. Opt.*, vol. 18, 2016, Art. no. 085503.

[19] D. D. Hickstein *et al.*, "High-harmonic generation in periodically poled waveguides," *Optica*, vol. 4, no. 12, pp. 1538–1544, 2017.

[20] T. Kishimoto, K. Inafune, Y. Ogawa, H. Sasaki, and H. Murai, "Highly efficient phase-sensitive parametric gain in periodically poled $LiNbO_3$ ridge waveguide," *Opt. Lett.*, vol. 41, no. 9, pp. 1905–1908, 2016.

[21] X. F. Chen, J. H. Shi, Y. P. Chen, Y. M. Zhu, Y. X. Xia, and Y. L. Chen, "Electro-optic Solc-type wavelength filter in periodically poled lithium niobate," *Opt. Lett.*, vol. 28, no. 21, pp. 2115–2117, 2003.

[22] K. Liu, J. H. Shi, and X. F. Chen, "Linear polarization-state generator with high precision in periodically poled lithium niobate," *Appl. Phys. Lett.*, vol. 94, 2009, Art. no. 101106.

[23] K. Liu, W. J. Lu, Y. P. Chen, and X. F. Chen, "Active control of group velocity by use of folded dielectric axes structures," *Appl. Phys. Lett.*, vol. 97, 2010, Art. no. 071104.

[24] C. Y. Huang, C. H. Lin, Y. H. Chen, and Y. C. Huang, "Electro-optic Ti:PPLN waveguide as efficient optical wavelength filter and polarization mode converter," *Opt. Express*, vol. 15, no. 5, pp. 2548–2554, 2007.

[25] A. Rao and S. Fathpour, "Compact lithium niobate electrooptic modulators," *IEEE J. Sel. Top. Quantum Electron.*, vol. 24, no. 4, 2018, Art. no. 3400114.

[26] N. Courjal *et al.*, "High aspect ratio lithium niobate ridge waveguides fabricated by optical grade dicing," *J. Phys. D*, vol. 44, 2011, Art. no. 305101.

[27] A. Caspar *et al.*, "High-aspect-ratio $LiNbO_3$ ridge waveguide with vertical buffer layer and enhanced electro-optical efficiency," *J. Lightw. Technol.*, vol. 36, no. 13, pp. 2702–2707, Jul. 2018.

[28] A. J. Mercante, D. L. K. Eng, M. Konkol, P. Yao, S. Shi, and D. W. Prather, "Thin $LiNbO_3$ on insulator electro-optic modulator," *Opt. Lett.*, vol. 41, no. 5, pp. 867–869, 2016.

[29] K. Liu, J.-H. Shi, Z.-E. Zhou, and X.-F. Chen, "Electro-optic Solc-type flat-top bandpass filter based on periodically poled lithium niobate," *Opt. Commun.*, vol. 282, pp. 1207–1211, 2009.

[30] K. Liu, J.-H. Shi, and X.-F. Chen, "Electro-optical flat-top bandpass Solc-type filter in periodically poled lithium niobate," *Opt. Lett.*, vol. 34, no. 7, pp. 1051–1053, 2009.

Tingting Ding received the B.S. degree from the Minzu University of China, Beijing, China, in 2015. She is currently working toward the Ph.D. degree under the supervision of X. Chen with the School of Physics and Astronomy, Shanghai Jiao Tong University, Shanghai, China. Her research interests include nonlinear optics and micro/nano integrated photonics on lithium niobate-on-insulator platform.

Yuanlin Zheng received the B.S. and Ph.D. degrees from Shanghai Jiao Tong University (SJTU), Shanghai, China, in 2008 and 2013, respectively. From 2013 to 2015, he was a Postdoctoral Research Fellow with the School of Physics and Astronomy, SJTU, where he is currently an Assistant Researcher. His research interests include nonlinear optics, micro/nano integrated photonics, and optical cavities.

Xianfeng Chen received the Ph.D. degree in optics from Shanghai Jiao Tong University (SJTU), Shanghai, China, in 1999. He is currently a Distinguished Professor with the School of Physics and Astronomy, SJTU. He has published more than 200 refereed journal articles. During the past decade, his researchers have focused on nonlinear optics, nano photonics, laser physics and technology, etc. He received the China National Funds for Distinguished Young Scientists in 2011 and the C. N. Yang Award from AAPPS for the contribution to quasi-phase-matching nonlinear optics in 2010.